Morphology and growth of carbon nanotubes catalytically synthesised by premixed hydrocarbon-rich flames

Cheng Tung Chong,[a,b,*], Win Hon Tan[a], Siew Ling Lee[c], William Woei Fong Chong[a,b], Su Shiung Lam[d], Agustin Valera-Medina[e]

[a] Faculty of Mechanical Engineering, Universiti Teknologi Malaysia 81310 Skudai, Johor, Malaysia.
[b] UTM Centre for Low Carbon Transport in cooperation with Imperial College London, Universiti Teknologi Malaysia, 81310 Skudai Johor, Malaysia.
[c] Centre for Sustainable Nanomaterials, Ibnu Sina Institute for Scientific and Industrial Research, Universiti Teknologi Malaysia 81310 Skudai Johor, Malaysia.
[d] Eastern Corridor Renewable Energy Group (ECRE), Environmental Technology Programme, School of Ocean Engineering, Universiti Malaysia Terengganu, 21030 Kuala Terengganu, Terengganu, Malaysia.
[e] College of Physical Sciences and Engineering Cardiff University, Wales, UK.

Abstract

Synthesis of carbon nanotubes (CNTs) was performed by using a laminar premixed flame burner at open atmospheric condition. The growth of CNTs on the substrate was supported catalytically by a transition metal under high temperature, hydrocarbon-rich environment. Analysis of the CNTs using high resolution electron microscope reveals the structure of synthesised nano-materials in disarray, clustered and tubular form. The graphitic structure of the CNTs are rather similar for all fuel-rich equivalence ratios tested, with an average diameter of ~11-13 nm. Removal of the amorphous carbon and catalyst in the CNTs was performed via purification treatment using H_2O_2 and HCl solutions. Detail characterisation indicates the oxidation temperature of purified CNTs ranges between 497-529 °C. Deconvolution of the Raman spectra in the range of 900-1800 cm^{-1} into five components show the distinct characteristic bands of CNTs with I_G/I_D ratio of 0.66-0.72 for all the samples tested. In addition, the high level carbon concentration and sp^2 C-C bond in the CNTs was validated by X-ray photoelectron spectroscopy analysis. The present study demonstrates that CNTs can be effectively synthesised from fuel-rich hydrocarbon flames at ϕ=1.8-2.0 supported by nickel-based substrate.

Keywords: Carbon nanotubes, flame synthesis, Raman spectroscopy, TEM, CNT morphology, XPS

*Corresponding author
Address: Faculty of Mechanical Engineering Universiti Teknologi Malaysia 81310 Skudai Johor, Malaysia.
Email: ctchong@mail.fkm.utm.my ; Phone: +60(7) 5534631 ; Fax: +60 (7) 5566159

1.0 Introduction

Carbon nanotubes (CNTs) are sheets of graphene rolled into tubular form. A single-wall carbon nanotube (SWCNT) is defined as single graphene sheet of nanotube, while a multi-wall carbon nanotube (MWCNT) consists of two or more graphene sheets of nanotubes [1]. CNTs have a mechanical strength 10 times greater than steel even though the density is 1/6 of the latter due to the existence of sp^2 C-C bonds [2]. Additionally, CNTs are flexible [3] and could withstand buckling under compression. The thermal conductivity of CNT is approximately 6600 W/mK [4]. The superior properties of CNTs allow diverse applications in products such as enhanced composite materials [5, 6], batteries [7, 8], ultra-capacitors [9] and biosensors [10]. The high demand for CNTs prompts for techniques to synthesise CNTs at economical scale.

Flame synthesis is a potential method that could be utilised to produce CNTs owing to the high temperature and carbon-rich environment [11]. This condition is desirable for CNT formation if transition metal catalyst such as Fe, Co and Ni is present. Flame synthesis is a continuous-flow, scalable method with potential for considerably lower cost of production of CNTs compared to other methods, such as those of chemical vapour deposition (CVD) [12], laser ablation [13] and arc discharge [14] methods. Observation of carbon in tubular structure produced by premixed flames was first reported by Singer and Grumer [15]. Since then, different flame configurations have been used for CNT synthesis, including normal diffusion, inverse diffusion, counter-flow, and premixed flames [16]. Vander Wal [17] demonstrated the growth of CNTs by using a normal diffusion flame supported by TiO_2 catalyst. Hu *et al.* [18] managed to synthesise well-aligned MWCNTs by using an ethylene diffusion flame on a thin-film anodic aluminium oxide (AAO) template coated with cobalt. The CNTs synthesised were strongly bonded to the substrate and well-graphitised. It was reported that the diameter and length of the CNTs can be controlled via the template. Camacho *et al.* [19] carried out flame

synthesis of carbon nanostructures with diffusion flame established by methane, propane and acetylene. Galvanized steel wire mesh was used as substrate. Results showed that methane diffusion flame produced thin MWCNTs, nanorods and nanofibers, while propane diffusion flame yielded nanotubes. The products synthesised by acetylene diffusion flame were helically coiled and twisted nanotubes. The oxidation temperature of the synthesised products ranged between 610 - 712 °C.

Yuan *et al.* [20] reported the synthesis of MWCNTs using a normal diffusion flame. The fuel source used was methane, supplied through a 1.1 cm diameter of stainless-steel tube and surrounded by a co-flow air. A Ni/Cr wire was inserted into the flame and held for 15-30 minutes. The optimum CNT yield was found to locate at around one-fifth to one-third of the total flame height (65 cm). Post-synthesis analysis revealed that the wire contained MWCNTs with diameters between 20 to 60 nm. In another related study, Yuan *et al*. [21] utilised the same burner but ethylene fuel was used. Results showed that dilution of gaseous hydrocarbon fuels with nitrogen led to the production of aligned MWCNTs. This could be due to the lower flame temperature when nitrogen was introduced. Another experiment conducted by Yuan *et al.* [22] showed that Ni-Cr-Fe wire oxidised using nitric acid led to the increase of CNT yield. They proposed a three-step mechanism of CNT growth via diffusion flame synthesis method. The metal catalyst first oxidised to form metal oxides in the flame, enabling carbon species to be absorbed on the catalyst surface to form carbon precursors. The carbon atoms then diffused into the catalyst and precipitated to form CNTs.

Lee *et al.* [23, 24] reported the growth of MWCNTs by using an inverse ethylene diffusion flame. The inner tube used to supply air had a diameter of 11 mm, while the outer tube supplying nitrogen and ethylene had a diameter of 94 mm. A stainless steel plate coated with $Ni(NO_3)_2$ was used as substrate for CNT growth. Unlike normal diffusion flames, the fuel-rich condition was outside the flame front, hence the formation of CNTs was observed at the

range of 5 to 7 mm from the flame centre in the radial direction. The formation of MWCNTs was mostly observed in the region with temperature range of 1000 to 1300 K, while the formation of nanofibers was observed at a lower temperature range of 800 to 1000 K. Xu *et al.* [25] demonstrated the growth of well-aligned MWCNTs using methane inverse diffusion flames. Spontaneous Raman spectroscopy was used to monitor the local gas-phase temperature and carbon-based species. Result showed that the growth of CNTs was sensitive to substrate composition, sampling position, temperature and species concentration. Vertically well-aligned CNTs with uniform diameter of 15 nm were grown, and optimal CNT growth in regions outside the visible soot/precursor luminescence was reported.

Premixed flame is established by mixing fuel and oxidiser prior to ignition at the burner outlet. Duan and McKinnon [26] synthesised CNTs by using premixed benzene-air flame at low pressure condition and observed the growth of MWCNTs with significant amount of amorphous soot. Howard *et al.* [27] also managed to observe CNTs and nano-particles synthesised via a premixed flame configuration with acetylene and benzene as fuel sources. Chowdhury *et al.* [28] extended the investigation by using various fuel source including benzene, acetylene and ethylene (diluted with argon) to premix with air at low pressure environment. Results showed that the size of produced MWCNTs ranged between 2 - 30 nm with internal diameters of 1 - 10 nm.

Vander Wal *et al.* [29] managed to synthesise CNTs by using a high temperature tube furnace with premixed flames supported by Fe and Ni catalysts. By premixing CO/H_2 with air and utilising Fe as catalyst, SWCNTs were produced. MWCNTs were produced when C_2H_2/H_2/air flame was established and nickel was used as catalyst. In another related study by the same group, the effect of fuel source on the growth of CNTs were investigated by using premixed flames [30]. The growth of MWCNTs was observed by using ethane, ethylene, acetylene, and propane fuel-rich flame. Cobalt was used as catalyst and coated to a stainless

steel substrate. Interestingly, no CNTs were observed for methane flames established at fuel rich conditions of $\phi = 1.5$ to 2, probably due to the lack of carbon precursor, contrary to the results reported by using a methane diffusion flames [31].

Goel *et al.* [32] compared the growth of CNTs by using premixed and diffusion flames with benzene as hydrocarbon sources. It was reported that diffusion flame resulted in higher yield of CNTs compared to premixed flames. The growth of CNTs is strongly affected by the residence time for premixed flames. Woo *et al.* [33] utilised a double-face wall stagnation flow burner to synthesise CNTs with ethylene as fuel and nickel as catalyst. MWCNTs were observed to grow on the substrate. The experiment highlighted that CNT growth is sensitive to mixture's equivalence ratio at high stretch rate conditions. Height *et al*. [34] utilised premixed acetylene flame supported by iron pentacarbonyl catalyst to grow SWCNTs. CNT was formed at the temperature range between 1500 and 1800 K and at equivalence ratios of $\phi = 1.5$ - 1.9. The diameter of the individual CNT ranges between 0.9 and 1.5 nm. Diener *et al.* [35] concurred that acetylene and ethylene were suitable for synthesising SWCNTs while benzene was effective in producing MWCNTs.

Flame synthesis has been shown effective in synthesising CNTs without both large setup cost and huge energy input [36]. Due to variation in flame configuration, operating condition and fuel source, the morphology, structure and overall quality of CNTs produced would vary and require detailed characterisation. Previous investigations have focused on visual characterisation using electron microscope. In this experiment, the CNTs synthesised by premixed flames are characterised in detailed. The effect of mixture's equivalence ratio on the growth and morphology of CNTs is investigated.

2.0 Experimental

The experimental setup for CNT synthesis is shown in Figure 1. A premixed flame burner was utilised to establish an open, cone-shaped flame at atmospheric condition. The burner body is cylindrical in shape, with inner tube diameter of 70 mm and height of 350 mm, while the contoured nozzle outlet is 20 mm in diameter. Propane was employed as fuel source to premix with air to establish a fuel-rich flame, providing the carbon source for CNT growth [37]. Two mass flow controllers (Sierra; SmartTrack50, ±1% accuracy) were utilised to regulate the mass flow of air and fuel supplies. Nano-sized nickel catalyst (Sigma-Aldrich; 65 wt % nickel) was coated on a substrate of stainless steel wire mesh (10 x 10 cm) placed above the premixed burner for CNT growth. The mesh number of the substrate is 80. The distance between the burner nozzle outlet and the substrate was fixed at 10 cm. The fuel/air ratio is defined in terms of a non-dimensional variable known as equivalence ratio ϕ, which is the ratio of the actual fuel-to-oxidizer ratio normalized by the stoichiometric fuel-to-oxidizer ratio: $\phi = (F/A)_{actual} / (F/A)_{stoichiometric}$, where F is the number of moles of fuel, A is the number of moles of air. Stoichiometric fuel/air mixture is denoted as $\phi = 1$, whereas fuel–lean and fuel-rich mixtures are denoted as $\phi < 1$ and $\phi > 1$, respectively. In the present study, the air-fuel was varied between the equivalence ratios of $\phi = 1.8$ and 2.2. The synthesis time for all test cases was 15 minutes. The operating conditions are shown in Table 1.

Commented [AVM1]: Probably redundant for the audience?

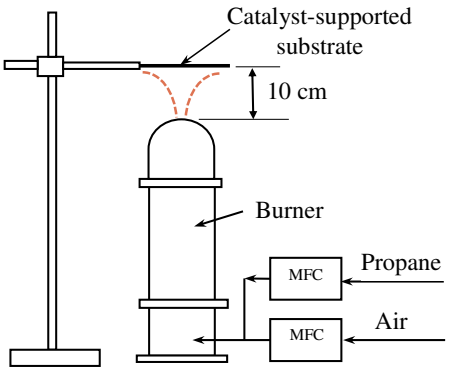

MFC= mass flow controller

Figure 1: Schematic of experimental setup for CNT flame synthesis.

Table 1: Operating conditions

Equivalence ratio ϕ	Propane mass flow rate, $\dot{m}_f$ (g/s)	Air mass flow rate, $\dot{m}_a$ (g/s)
1.8	0.09	0.75
2.0	0.09	0.74
2.2	0.10	0.73

2.1 Post-synthesis purification treatment

The raw CNTs synthesised by flame was purified to remove impurities such as nickel particles and amorphous carbon prior to characterisation. The CNTs were purified by immersing them in 30% hydrogen peroxide (H_2O_2) for 24 hours, followed by immersion in hydrochloric acid (HCl) for 24 hours [38]. H_2O_2 is an effective oxidising agent used to remove amorphous carbon [39] while HCl dissolves the nickel catalyst deposited on the CNT surface [40]. A magnetic stirrer was used to ensure the CNTs are well immersed and mixed in the solution. A filter paper was used to separate the CNTs from the solution. Distilled water was used to rinse the CNTs until pH 7 was reached.

2.2 Characterisations of CNTs

The equipment utilised to provide qualitative and quantitative information on the CNTs synthesised are described in the following subsections.

2.2.1 Scanning electron microscopy (SEM) and Energy dispersive X-ray spectroscopy (EDX)

A field electron scanning electron microscope (JEOL JSM-6701F) coupled with energy X-ray spectroscopy (EDX) was used to observe the surface morphology of synthesised CNTs and to determine the elements present in the sample. CNT samples collected from the substrate were purified before being placed on a carbon conductive tape for analysis.

2.2.2 Transmission electron microscopy (TEM)

A TEM (Hitachi; model: HT7700) was used to characterise the structural properties and identify the inner morphology of CNTs. The TEM was operated at 120 kV accelerating voltage and high-resolution mode to image the micrograph of CNTs. Prior to TEM imaging, a small amount of CNTs sample was dispersed in 1 ml of methanol. The methanol was immersed in an ultrasonic bath for 2 hours to prevent agglomeration of CNTs. A copper grid mesh with mesh number 300 (ProSciTech; model: GSCU300FL) was immersed in the methanol solution for few seconds and dried before inserting into the specimen rod. The TEM micrographs were used to measure the external diameter, internal diameter and interlayer spacing of CNTs. The diameters of CNTs were measured based on the average value of 100 individual CNTs. The interlayer spacing was measured based on the grey value of line profile across the wall of CNT.

2.2.3 X-ray powder diffraction (XRD)

X-ray power diffraction (XRD) provides information about the structure of crystalline materials. An XRD (Rigaku; model: HyPix-3000) was used in the present experiment to characterise the synthesised CNTs. A Cu X-ray source Kα (λ=0.154 nm), monochromated radiation was used. The CNTs samples were scanned for the range of 2° to 100° (2θ angle) with 0.02° step.

2.2.5 Raman analysis

Raman spectrum analysis provides signature spectrum for all types of carbon allotrope. A Raman spectroscopy system (HORIBA; model: XploRA PLUS) was used in the present study. Raman analysis was performed with a 532 nm wavelength laser and the spectrum was recorded under standard atmospheric condition. The analysis was done by placing the CNT

sample on a glass substrate, and the Raman spectra were recorded from 100 - 4000 cm^{-1}. Each spectrum was recorded for a duration of 30 s with 20 scans.

2.2.6 Thermogravimetric analysis (TGA)

Thermogravimetric analysis (TGA) is used to characterise the thermal properties of carbonaceous materials. A thermogravimetric analyser (TA Instruments; model: Q500) coupled with a FT-IR spectrometer (Nicolet iS10) was used in present study. 10 mg of CNTs sample was heated from room temperature to 900 °C at heating rate of 10 °C/min with air flowing at 60 cm^3/min. Parameters such as the initial oxidation temperature (T_i), oxidation temperature (T_o) and residue weight were determined from the weight loss curve and first derivative of weight loss curve.

2.2.7 X-ray photoelectron spectroscopy (XPS)

X-ray photoelectron spectroscopy (XPS) is utilised to obtain information related to elemental compositions and functional groups on the material surface. An XPS equipment (Shimadzul; model: AXIS Ultra DLD) was used to detect the functional group of purified CNTs. The XPS test was conducted by using a standard aluminium X-ray anode (150 W) to generate photoelectron in vacuum environment. Pass energy, energy step and Dwell time were set to 160 eV, 1 eV and 100 ms respectively. The functional groups attached in the CNT sample was determined via peak fitting technique.

3.0 Results and discussion

3.1 Morphology of CNTs

Post-flame synthesis observation of the substrate shows that at region I, high density of CNTs grew on the surface of the substrate impinged by the luminous premixed flame zone. The CNTs formed are in disarray and in random direction, as shown in the FESEM micrograph magnified at x 5k in Figure 2b. In this region, the bluish flame that impinges the substrate is the main reaction zone where excited CH* radicals were radiated. The main reaction zone is where the flame front locates with the highest temperature, thus allowing high diffusional rate of carbon into the transition metal catalyst [41]. Within the flame reaction zone, intermediate product gases are formed during homogenous gas phase reactions. The main gas precursors that promote the formation of nano-structured solid carbon are hydrocarbon (C_nH_m) and carbon monoxide (CO). Hydrocarbon decomposes at high temperature to form solid carbon. Carbon monoxide participates in deposition of solid carbon via Boudard reaction ($2CO_{(g)} \leftrightarrow C_{(s)} + CO_{2(g)}$ ΔH= -171 kJ/mol) and hydrogenation reaction ($CO + H_2 \leftrightarrow C_{(s)} + H_2O$ $\Delta H = -131$ kJ/mol) [16]. Propane fuel undergoes pyrolysis process during reaction and produces acetylene. Acetylene reacts with other radicals to become polyacetylenes or polyacetylenic radical. Through cyclization process, polynuclear aromatic hydrocarbon (PAH) is formed. These PAH then stacks up in platelet to form CNTs in the presence of catalyst. Without catalyst, the PAH will form soot in agglomerated form [42]. In region II, no CNTs were observed, only nickel particles in nanoscale (Figure 2c) coated on the substrate surface. This region is the pre-reaction zone where no reaction takes place. The fuel/air mixture was fed into the reaction zone (region I) for further chemical reaction.

Commented [AVM2]: Question. Isn't the blue part where OH* forms, and the yellowish the one that shows the CH* luminescence (soot)?

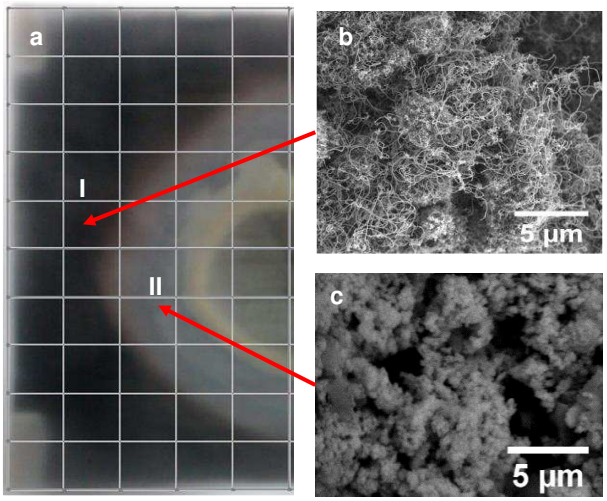

Figure 2: (a) Distribution of CNTs on a substrate (50 mm x 100 mm) after flame synthesis process and micrograph of (b) CNTs deposited on substrate (region I), magnified at x5 K and (c) nickel catalyst that is unreacted (region II). Flame synthesis was performed at $\phi = 2.0$.

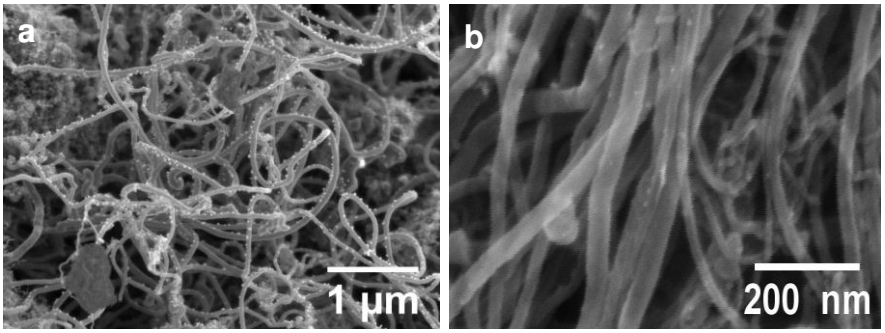

Figure 3: FESEM micrographs of (a) raw CNTs grew on the substrate magnified at x25 K and (b) post-treated CNTs magnified at x 100 K. Flame synthesis was performed at $\phi = 2.0$.

FESEM imaging of the raw CNTs magnified at x25 K is shown in Figure 3a. Particles of nickel were observed to deposit on the surface of CNTs. This is due to the high temperature

environment in the flame region that caused the nickel (T_{melt} = 1450 ^{o}C) to melt and deposited on the CNT surface to form small particles. The particles on the CNTs were confirmed by EDX point-based analysis which shows high level of nickel. EDX analysis performed on the bulk raw CNT sample shows that carbon content is approximately 82.7% wt, while nickel content is about 9.9% wt. Other trace elements detected in the sample are Si, Al, O, which originate from the catalyst used. Nickel is reactive towards C_2H_2, coupled with particle size of 5 nm and above, the formation of CNTs is favourable. Konya et al. [43] reported that nickel is effective in synthesising well-graphitised carbon nanotubes. The level of purity of CNTs can be increased via post-treatment of using HCl solution to remove the nickel particles. Figure 3b shows the post-treated CNTs magnified at x100 K.

3.2 TEM micrographs of CNT structures

The CNTs were observed to be long, cylindrical in shape and hollow in the middle of the tube. The CNTs' physical appearance is in disarray, often in entangled form with different bends and curvatures due to their long structural length, as shown in Fig. 4a. High-resolution TEM micrograph shows that catalyst particles are encapsulated by the graphitic structure and located at the tip of CNTs, as shown in Fig. 4b. Based on the vapour-liquid-solid mechanism, the carbon radical species produced during decomposition of propane are absorbed on the surface of the nickel catalysts, followed by bulk diffusion of carbon atom into the metal catalysts. When liquid metastable carbide reaches supersaturated stage, solid carbon precipitates to form CNTs [44]. The measured temperature on the substrate during synthesis of CNTs were in the range of 869 – 1014 °C, which is favourable for carbon deposition due to gas-solid interactions. Figure 4c shows the micrograph of amorphous carbon in the samples. Amorphous carbon encapsulates the nickel particles, leading to catalyst deactivation and subsequently prohibits the formation of CNTs [16].

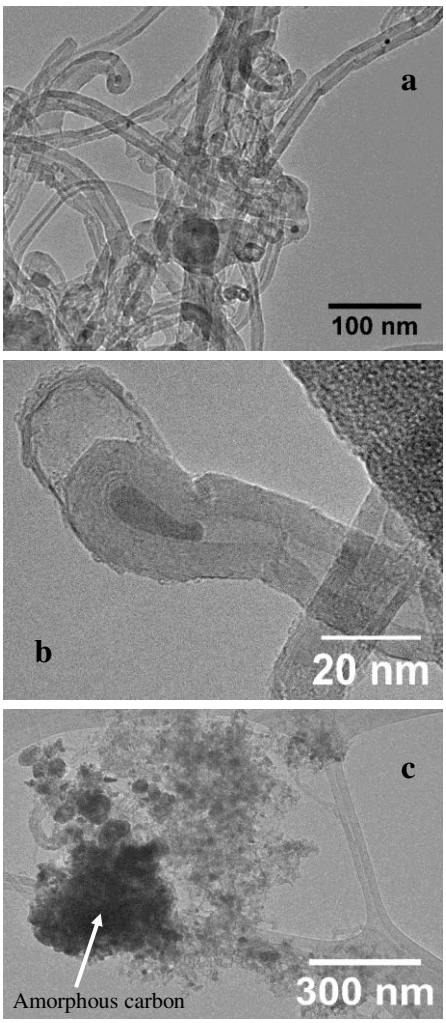

Figure 4: High resolution TEM images of (a) CNTs in disarray form, (b) nickel catalyst encapsulated by graphitic structure at the tip of CNT and (c) amorphous carbon formed in the sample. The CNTs were synthesised at $\phi = 2.0$.

3.3 Effect of equivalence ratio on growth of CNTs

3.3.1 TEM imaging and analysis

The CNTs produced from rich propane/air flame with equivalence ratios of ϕ = 1.8, 2.0 and 2.2 are shown in Figure 5a, b and c, respectively. The clusters of CNTs synthesised at ϕ =1.8 is not as dense as ϕ=2.0 and 2.2, which is expected as fuel-richer flame contains higher amount of carbon content. Closer examination of the CNT structure reveals well-defined (0 0 2) lattice fringes, as evidenced in the TEM micrographs of Fig 5d, e and f, which are independent of the mixture's equivalence ratio. The structure shows CNTs that consist of layers of wall. The average tube wall diameters derived from 100 samples are 12.3, 12.1 and 11.3 nm, with standard deviations of 4.87, 5.68 and 5.21 nm for ϕ = 1.8, 2.0 and 2.2 respectively. The d_{200} values obtained from the grey scale profile across lattice structures are 0.31 nm, 0.32 nm and 0.32 nm for ϕ= 1.8, 2.0 and 2.2 respectively, as shown in Fig. 5g, h and i. The present interlayer spacing values of CNTs are comparable to those derived from the chemical vapour deposition method, which are in the range of 0.32-0.35 nm [45]. Results show the consistency of the CNTs' structure obtained regardless of the mixtures' equivalence ratios.

Commented [AVM3]: Didn't understand this part. Layers of wall?

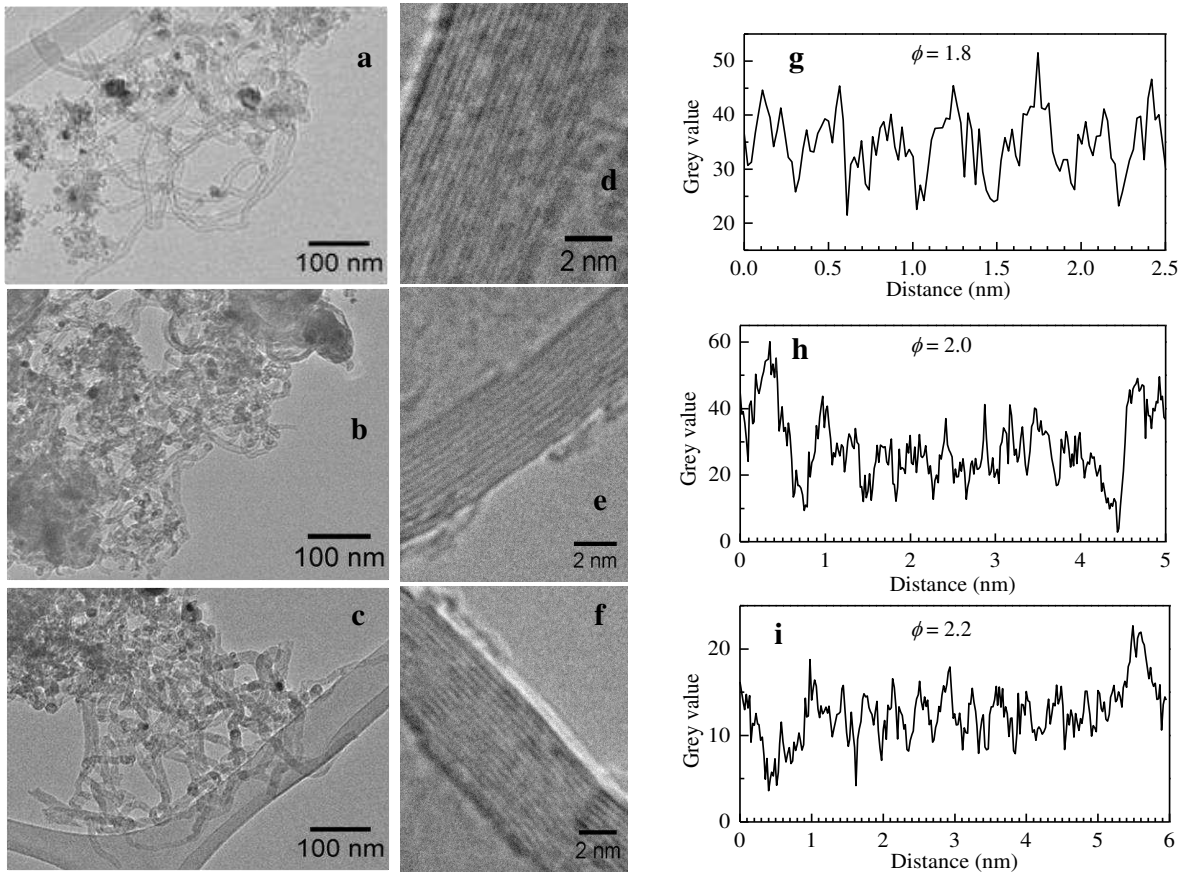

Figure 5: High resolution TEM micrographs of CNTs synthesised with premixed propane/air at ϕ = (a, d) 1.8, (b, e) 2.0 and (c, f) 2.2 and the corresponding grey scale profiles across CNT wall.

3.3.2 XRD analysis

The XRD spectra of raw CNT sample synthesised at $\phi = 1.8$, 2.0 and 2.2 are shown in Fig. 6. In general, the XRD spectra for all cases show the pattern of nickel oxide, nickel carbide, nickel and CNTs. The peak appearing at 26.15° is the C(0 0 2) reflection of the hexagonal graphite structure, indicating the graphite structure of multi-wall CNTs. The sample shows the highest intensity of the graphite peak C (0 0 2) for $\phi = 2.0$, with a calculated interlayer spacing of 0.34 nm.

Comparison of the graphite peak shows that $\phi = 2.0$ exhibits the highest relative intensity and lowest nickel oxide peak intensity. The graphite structure peak for $\phi = 1.8$ is slightly lower than $\phi = 2.0$. The peak for graphite structure is located at 26.0° and the calculated interlayer spacing of graphite (2 0 0) is 0.342 nm. For mixture of $\phi = 2.2$, the relative intensity is evidently lower. The graphite structure peaks at 26.5° with the interlayer spacing of graphite (2 0 0) of 0.336 nm. At ultra-rich condition, the rate of hydrocarbon deposition to form PAH is higher than decomposition and dissolution in carbon. The PAH formed will deactivate the catalyst for CNT growth, leading to formation of amorphous carbon due to excess of carbon. During the flame synthesis process, oxygen reacts with the nickel particle catalyst to form nickel oxide. Formation of nickel oxide will impact CNT growth because nickel oxide does not dissolve carbon, leading to deactivation of the catalyst [46]. Despite the slight variation in graphite peak intensity, the overall spectra for all cases are almost similar.

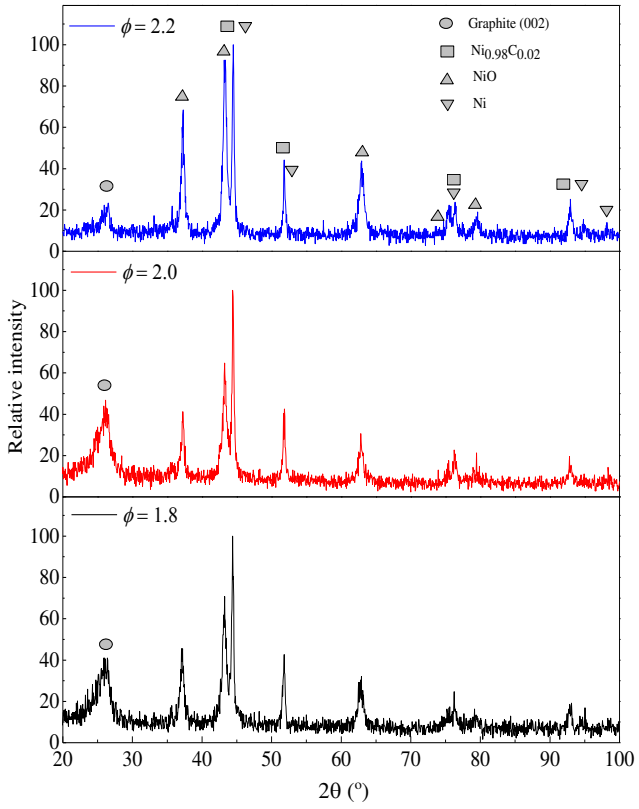

Figure 6: XRD patterns of CNTs sample synthesised at $\phi = 1.8$, 2.0 and 2.2.

3.2.3 TGA analysis

Thermogravimetric analysis (TGA) was used to analyse the thermal stability and purity of the CNT samples [47]. CNTs with higher oxidation temperature indicates higher crystallinity level [48]. The oxidation temperature of carbon depends on the level of graphitic structure. Figure 7 shows the weight loss curves and first derivatives of CNT samples synthesised at different equivalence ratios. Oxidation temperature of the samples can be divided into three

stages. At temperatures below 350 ºC, water content and some absorbed species are removed, resulting in weight loss in the sample; between 350 – 400 ºC, amorphous carbon and disordered carbon starts to oxidise. At temperatures above 400 °C, oxidation of amorphous carbon and CNTs occur simultaneously [49]. In the present study, oxidation of the sample starts at around 450 °C and completes at around 650 °C. The weight loss curve shows that CNT yield increases with the increase of equivalence ratio. The remaining residues after the oxidation process are 65%, 56%, and 42% for equivalence ratios ϕ = 1.8, 2.0 and 2.2 respectively, indicating a trend of decreasing residues with increasing equivalence ratio. At higher equivalence ratio (richer flame), the concentration of carbon species is higher, thus enabling higher rate of diffusivity of carbon into transition metal [50].

The weight loss graph shows CNT sample losses weight insignificantly before the main oxidation peak. This indicates that the presence of amorphous carbon is relatively less, as the amorphous carbon could have been oxidised in the flame during such a flame synthesis process, leaving the relatively stable graphitic materials which are CNTs. The first derivative of weight loss graph shows that all samples have oxidation temperatures of around 500 °C. The oxidation temperatures for CNTs synthesised at ϕ =1.8, 2.0 and 2.2 are 525°C, 529°C and 497°C respectively. Carbon yield increases with increasing equivalence ratio, but an ultra-rich (ϕ = 2.2) flame condition leads to poorer graphitic characteristic.

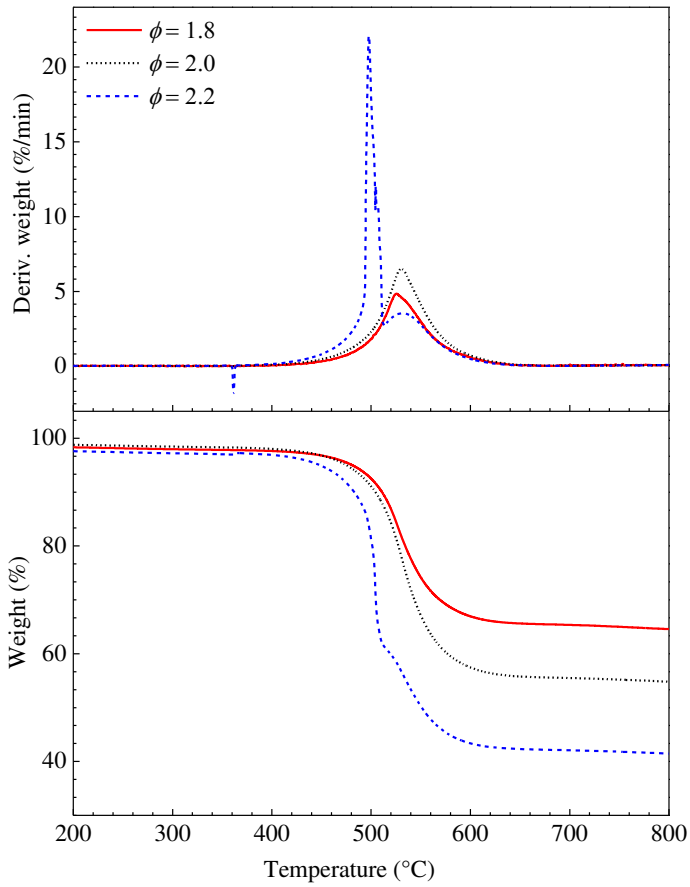

Figure 7: TGA of weight loss curves and the first derivative for CNTs samples synthesised at ϕ = 1.8, 2.0 and 2.2.

3.2.4 Raman spectroscopy analysis

The Raman spectra of untreated CNTs synthesised at various equivalence ratios are shown in Figure 8. The Raman spectrum for the present CNTs shows three characteristic peaks, namely D-band at 1340 cm^{-1}, G-band at 1582 cm^{-1} and G' at 2700 cm^{-1} for all the equivalence ratios tested, indicating the typical multi-wall CNTs' Raman spectrum [47]. The G and G' band in the Raman spectrum indicate the presence of graphitic sp^2 materials [51], while the D band is attributed to the presence of amorphous carbon and defect of CNTs [52]. The D' band is observed as the weak shoulder of G band at higher frequency. All carbon allotrope with sp^2 structure is reflected in the G' band peak that is in the range of 2500 cm^{-1}- 2800 cm^{-1} in the Raman spectra. The radial breathing modes at low frequency are not observed due to large diameter of the tubes [53]. Deconvolution of the spectra in the range of 900-1800 cm^{-1} into five Lorentzian peaks using Origin software is shown in Figure 9. The D' band located at ~1620 cm^{-1} is attributable to the presence of edge carbon atoms [54]. The D3 and D4 bands are shown in the range of ~1450-1500 cm^{-1} and ~1100-1200 cm^{-1}, respectively. The nature of D3 line is uncertain, with some researchers attributing it to stacking and turbostratic structures [54, 55]. The D4 band is attributed to amorphous impurities in graphite materials [56] or adsorbed ions [57]. The ratio of the G and D band intensity, I_G/I_D ratios, for the CNT samples synthesised at ϕ = 1.8, 2.0, and 2.2 are 0.72, 0.66 and 0.67 respectively, with ϕ=1.8 showing the highest crystallinity level.

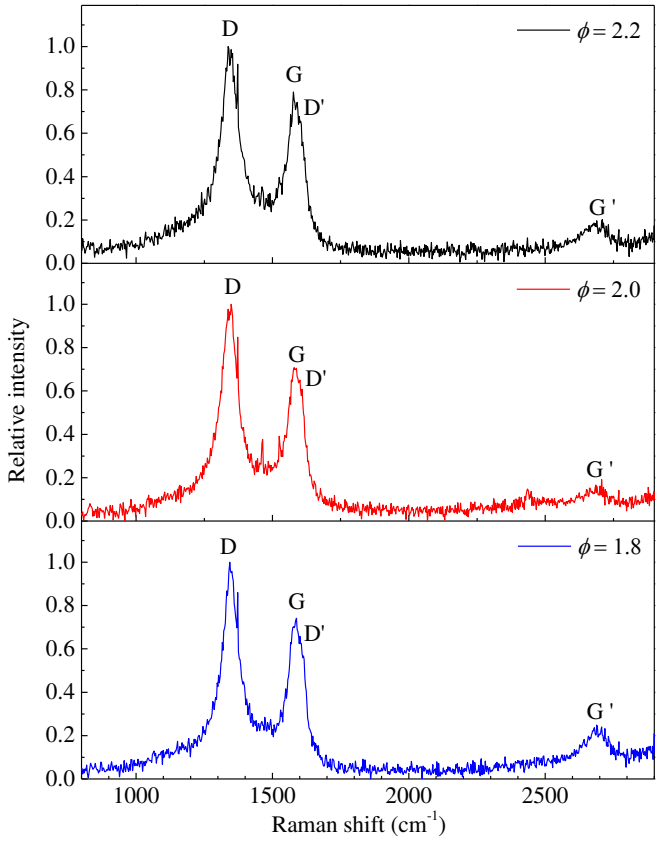

Figure 8: Raman spectra of CNTs samples synthesised at ϕ = 1.8, 2.0 and 2.2.

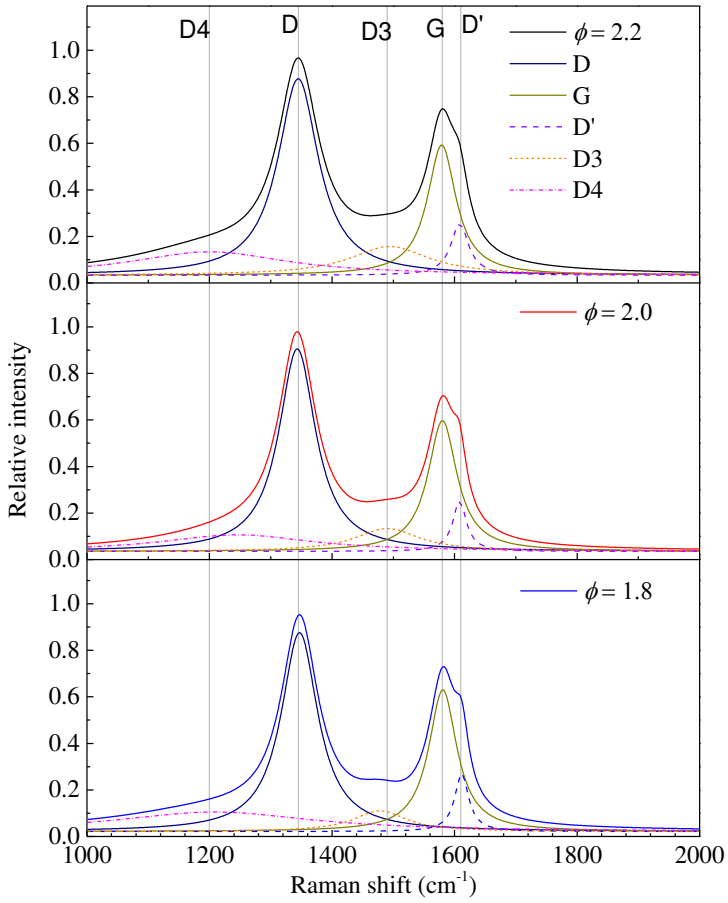

Figure 9: Deconvolution of Raman spectra into five Lorentzian peaks and band designations for CNTs synthesised at ϕ = 1.8, 2.0 and 2.2.

3.2.5 X-ray photoelectron spectroscopy analysis

XPS analyses elements on the surface and provides information on the functional groups of CNTs within the depth of < 10 nm. The XPS spectrum of purified CNT sample synthesised at ϕ=2.0 is shown in Figure 10a, showing the presence of carbon, oxygen and insignificant amount of silicon with the percentages of atomic concentrations of 88.3%, 10.9%, and 0.8% respectively (Table 2). The high percentage of carbon concentration indicates the effectiveness of purification process. No nickel catalyst was detected, as the catalyst particles on the surface were removed by purification process, while those covered by the graphitic structure were not detected by the surface analysis. Peak fitting performed on spectrally deconvoluted C(1s) peak provides information on the functional groups of the CNTs, as shown in Table 3. The overall peak in the range of 283-292 eV could be fitted by six peaks, as shown in Fig. 10b. The highest binding-energy peak (284.4 eV) in C1s is attributed to the sp^2 C-C bond, while the other five peaks are non-tubular carbon structure (285.6 eV), C-O (286.2 eV), -O-C=O (287.5 eV), carbonates group (289.3 eV) and π-π^* (291.0 eV). The XPS spectra confirms the attachment of functional groups with the peaks at 286.2, 287.5 and 289.3 eV, corresponding to carbon atoms attached to different oxygen-containing moieties and the π–π transition loss peak was detected at 291.0 eV. The peak at 285.6 eV is attributed to defects on the nanotube structure, which is relatively insignificant (< 5%) [38, 58]. Result shows that the CNTs contain high level of sp^2 carbon structure with low concentration of oxygen-containing functional groups.

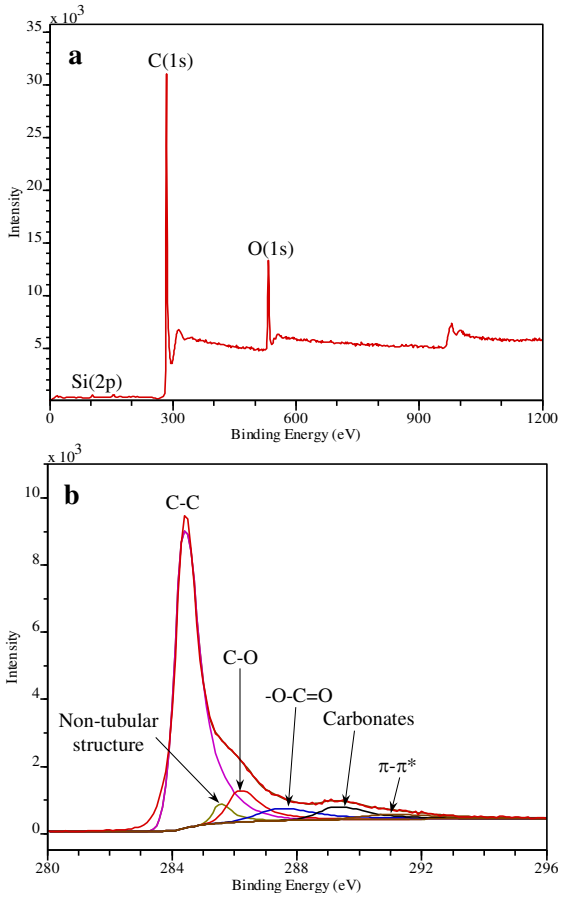

Figure 10: XPS spectra of (a) purified CNTs and (b) functional groups of C1(s) derived from peak fitting. The CNTs are synthesised at $\phi = 2.0$.

Table 2: XPS analysis results for purified CNTs

Elements	Position (eV)	FWHM	% Area
C (1s)	284.0	2.75	88.3
O (1s)	533.0	3.83	10.9
Si (2p)	103.0	4.27	0.81

Table 3: Functional groups of CNTs derived from peak fitting C(1s) peak

Functional group	Position (eV)	% Area
C-C	284.4	71.3
Non-tubular structure	285.6	4.0
C-O	286.2	9.1
-O-C=O	287.5	6.3
Carbonates	289.3	6.1
π-π^*	291.0	3.2

4.0 Conclusion

The structure and morphology of CNTs synthesised by propane flame premixed with air at fuel-rich equivalence ratios of ϕ=1.8-2.2 was examined. CNTs were observed to grow on substrate area impinged by the flame where abundant carbon species in the flame diffused into the transition metal catalyst before precipitating to form CNTs. Characterisation of the CNT structure shows layers of wall in the tube with rather uniform tube diameter in the range of 11-12.5 nm. The d_{200} value obtained from grey scale profile across lattice structures was of ~0.32 nm. X-ray diffraction analysis shows the graphite structure peaks at ~26.0°-26.5°, with an interlayer spacing of graphite (2 0 0) of 0.33-0.34 nm. Although amorphous carbon and nickels were observed to be present in the CNTs, purification treatment utilising H_2O_2 and HCl solutions was applied to remove impurities. TGA analysis shows that increasing equivalence ratio led to higher CNT yield owing to the increase of carbon content in the flame, with the oxidation temperature of CNTs ranging between 497-529 ^oC for all tested cases. The Raman spectra analysis reveals the typical spectra of multi-wall CNTs, denoted by the distinct D and G bands. Deconvolution the Raman spectra in the range of 900-1800 cm-1 into five Lorentzian peaks further shows the D', D3 and D4 bands. The relative intensity ratio of the G and D band, I_G/I_D ratio, are in the range of 0.66-0.72 for all samples, with ϕ=1.8 showing highest graphitic level. Surface analysis conducted via XPS shows the CNTs contain carbon concentration of 88.3% with high level of sp^2 C-C bond. The findings show that equivalence ratio of ϕ=1.8-2.0 tend to produce well-graphitised CNTs, indicating the potential of premixed hydrocarbon-rich flame as alternative method for synthesising CNTs.

Acknowledgement

The financial support from the Ministry of Higher Education Malaysia and Universiti Teknologi Malaysia (Research university flagship grant, vot no.: 03G63) is gratefully acknowledged.

References

[1] E.T. Thostenson, Z. Ren, and T. Chou, Advances in the science and technology of carbon nanotubes and their composites: a review, Composites science and technology. 61 (2001) 1899-1912.

[2] M.S. Dresselhaus, G. Dresselhaus, and P.C. Eklund, *Science of fullerenes and carbon nanotubes: their properties and applications*: Academic press, 1996.

[3] R.S. Ruoff and D.C. Lorents, Mechanical and thermal properties of carbon nanotubes, carbon. 33 (1995) 925-930.

[4] S. Berber, Y. Kwon, and D. Tománek, Unusually high thermal conductivity of carbon nanotubes, Physical review letters. 84 (2000) 4613.

[5] N. Zou and Q. Li, Compressive mechanical property of porous magnesium composites reinforced by carbon nanotubes, J. Material Sci. 51 (2016) 5232-5239.

[6] A. Ehsani, A. Vaziri-Rad, F. Babaei, and H. Mohammad Shiri, Electrosynthesis, optical modeling and electrocatalytic activity of Ni-MWCNT-PT nanocomposite film, Electrochimica Acta. 159 (2015) 140-148.

[7] Y.P. Wu, E. Rahm, and R. Holze, Carbon anode materials for lithium ion batteries, J. Power Sources. 114 (2003) 228-236.

[8] H. Huang, W.K. Zhang, X.P. Gan, C. Wang, and L. Zhang, Electrochemical investigation of TiO2/carbon nanotubes nanocomposite as anode materials for lithium-ion batteries, Materials Letters. 61 (2007) 296-299.

[9] Y. Che, H. Chen, H. Gui, J. Liu, B. Liu, and C. Zhou, Review of carbon nanotube nanoelectronics and macroelectronics, Semiconductor Science and Technology. 29 (2014) 073001.

[10] L. Dai, P. Soundarrajan, and T. Kim, Sensors and sensor arrays based on conjugated polymers and carbon nanotubes, Pure and Applied Chemistry. 74 (2002) 1753-1772.

[11] Y. Liu, C. Pan, and J. Wang, Raman spectra of carbon nanotubes and nanofibers prepared by ethanol flames, J. Material Sci. 39 (2004) 1091-1094.

[12] M. Kumar and Y. Ando, Chemical vapor deposition of carbon nanotubes: a review on growth mechanism and mass production, Journal of nanoscience and nanotechnology. 10 (2010) 3739-3758.

[13] C.D. Scott, S. Arepalli, P. Nikolaev, and R.E. Smalley, Growth mechanisms for single-wall carbon nanotubes in a laser-ablation process, Appl. Phys. A. 72 (2001) 573-580.

[14] J. Zhao, J. Zhang, Y. Su, Z. Yang, L. Wei, and Y. Zhang, Synthesis of straight multi-walled carbon nanotubes by arc discharge in air and their field emission properties, J. Material Sci. 47 (2012) 6535-6541.

[15] J.M. Singer and J. Grumer, "Carbon formation in very rich hydrocarbon-air flames—I. Studies of chemical content, temperature, ionization and particulate matter," in *Symposium (International) on Combustion*, 1958, pp. 559-569.

[16] J.P. Gore and A. Sane, Flame synthesis of carbon nanotubes, Carbon nanotubes-synthesis, characterization, applications. InTech. (2011) 122-32.

[17] R.L. Vander Wal, Flame synthesis of substrate-supported metal-catalyzed carbon nanotubes, Chemical Physics Letters. 324 (2000) 217-223.

[18] W. Hu, L. Yuan, Z. Chen, D. Gong, and K. Saito, Fabrication and characterization of vertically aligned carbon nanotubes on silicon substrates using porous alumina nanotemplates, Journal of nanoscience and nanotechnology. 2 (2002) 203-207.

[19] J. Camacho and A.R. Choudhuri, Effects of fuel compositions on the structure and yield of flame synthesized carbon nanotubes, Fullerenes, Nanotubes, and Carbon Nanostructures. 15 (2007) 99-111.

[20] L. Yuan, K. Saito, C. Pan, F.A. Williams, and A.S. Gordon, Nanotubes from methane flames, Chemical physics letters. 340 (2001) 237-241.

[21] L. Yuan, K. Saito, W. Hu, and Z. Chen, Ethylene flame synthesis of well-aligned multi-walled carbon nanotubes, Chemical physics letters. 346 (2001) 23-28.

[22] L. Yuan, T. Li, and K. Saito, Growth mechanism of carbon nanotubes in methane diffusion flames, Carbon. 41 (2003) 1889-1896.

[23] G.W. Lee, J. Jurng, and J. Hwang, Formation of Ni-catalyzed multiwalled carbon nanotubes and nanofibers on a substrate using an ethylene inverse diffusion flame, Combustion and flame. 139 (2004) 167-175.

[24] G.W. Lee, J. Jurng, and J. Hwang, Synthesis of carbon nanotubes on a catalytic metal substrate by using an ethylene inverse diffusion flame, Carbon. 42 (2004) 682–685.

[25] F. Xu, X. Liu, and D.T. Stephen, Synthesis of carbon nanotubes on metal alloy substrates with voltage bias in methane inverse diffusion flames, Carbon. 44 (2006) 570-577.

[26] H.M. Duan and J.T. McKinnon, Nanoclusters produced in flames, The Journal of Physical Chemistry. 98 (1994) 12815-12818.

[27] J.B. Howard, K.D. Chowdhury, and J.B.V. Sande, Carbon shells in flames, (1994)

[28] K. Chowdhury, J.B. Howard, and J.B. VanderSande, Fullerenic nanostructures in flames, Journal of materials research. 11 (1996) 341-347.

[29] R.L. Vander Wal and T.M. Ticich, Flame and furnace synthesis of single-walled and multi-walled carbon nanotubes and nanofibers, The Journal of Physical Chemistry B. 105 (2001) 10249-10256.

[30] R.L. Vander Wal, L.J. Hall, and G.M. Berger, Optimization of flame synthesis for carbon nanotubes using supported catalyst, The Journal of Physical Chemistry B. 106 (2002) 13122-13132.

[31] R.L. Vander Wal, L.J. Hall, and G.M. Berger, The chemistry of premixed flame synthesis of carbon nanotubes using supported catalysts, Proceedings of the Combustion Institute. 29 (2002) 1079-1085.

[32] A. Goel, P. Hebgen, J.B. Vander Sande, and J.B. Howard, Combustion synthesis of fullerenes and fullerenic nanostructures, Carbon. 40 (2002) 177-182.

[33] S.K. Woo, Y.T. Hong, and O.C. Kwon, Flame-synthesis limits and self-catalytic behavior of carbon nanotubes using a double-faced wall stagnation flow burner, Combustion and Flame. 156 (2009) 1983-1992.

[34] M.J. Height, J.B. Howard, J.W. Tester, and J.B. Vander Sande, Flame synthesis of single-walled carbon nanotubes, Carbon. 42 (2004) 2295-2307.

[35] M.D. Diener, N. Nichelson, and J.M. Alford, Synthesis of single-walled carbon nanotubes in flames, The Journal of Physical Chemistry B. 104 (2000) 9615-9620.

[36] W. Merchan-Merchan, A.V. Saveliev, L. Kennedy, and W.C. Jimenez, Combustion synthesis of carbon nanotubes and related nanostructures, Progress in Energy and Combustion Science. 36 (2010) 696-727.

[37] W.H. Tan, S.L. Lee, J.-H. Ng, W.W.F. Chong, and C.T. Chong, Characterization of carbon nanotubes synthesized from hydrocarbon-rich flame, International Journal of Technology. 7 (2016)

[38] V. Datsyuk, M. Kalyva, K. Papagelis, J. Parthenios, D. Tasis, A. Siokou, *et al.*, Chemical oxidation of multiwalled carbon nanotubes, Carbon. 46 (2008) 833-840.

[39] K. Hernadi, A. Siska, L. Thiên-Nga, L. Forró, and I. Kiricsi, Reactivity of different kinds of carbon during oxidative purification of catalytically prepared carbon nanotubes, Solid State Ionics. 141-142 (2001) 203-209.

[40] N.S. Gill, F.B. Taylor, W.E. Hatfield, W.E. Parker, C.S. Fountain, and F.L. Bunger, Tetrahalo Complexes of Dipositive Metals in the First Transition Series, in Inorganic Syntheses, Volume 9 (ed S. Y. Tyree), John Wiley & Sons, Inc., Hoboken, NJ, USA. . (1967)

[41] C.J. Lee, J. Park, Y. Huh, and J.Y. Lee, Temperature effect on the growth of carbon nanotubes using thermal chemical vapor deposition, Chemical Physics Letters. 343 (2001) 33-38.

[42] E.C. Zabetta and M. Hupa, Gas-born carbon particles generated by combustion: a review on the formation and relevance, Combustion and Materials chemistry. Biskopsgatan8, FIN-20500 Åbo, Finland. (2005)

[43] Z. Kónya, I. Vesselényi, J. Kiss, A. Farkas, A. Oszkó, and I. Kiricsi, XPS study of multiwall carbon nanotube synthesis on Ni-, V-, and Ni, V-ZSM-5 catalysts, Appl. Catalysis A: Gen. 260 (2004) 55-61.

[44] D. Yuan, "Property control of single walled carbon nanotubes and their devices," doctoral thesis, Duke University, 2008.

[45] O.V. Kharissova and B.I. Kharisov, Variations of interlayer spacing in carbon nanotubes, Rsc Advances. 4 (2014) 30807-30815.

[46] R.L. Vander Wal, T.M. Ticich, and V.E. Curtis, Diffusion flame synthesis of single-walled carbon nanotubes, Chemical Physics Letters. 323 (2000) 217-223.

[47] J.H. Lehman, M. Terrones, E. Mansfield, K.E. Hurst, and V. Meunier, Evaluating the characteristics of multiwall carbon nanotubes, Carbon. 49 (2011) 2581-2602.

[48] D. Bom, R. Andrews, D. Jacques, J. Anthony, B. hen, M.S. Meier, *et al.*, Thermogravimetric Analysis of the Oxidation of Multiwalled Carbon Nanotubes: Evidence for the Role of Defect Sites in Carbon Nanotube Chemistry, Nano Letters. 2 (2002) 615-619.

[49] C.S. Kumar, *Raman spectroscopy for nanomaterials characterization*: Springer Science & Business Media, 2012.

[50] P. De Bokx, A. Kock, E. Boellaard, W. Klop, and J.W. Geus, The formation of filamentous carbon on iron and nickel catalysts: I. Thermodynamics, Journal of catalysis. 96 (1985) 454-467.

[51] R.A. DiLeo, B.J. Landi, and R.P. Raffaelle, Purity assessment of multiwalled carbon nanotubes by Raman spectroscopy, Journal of Applied Physics. 101 (2007) 064307.

[52] R. Saito, A. Jorio, A.G. Souza Filho, G. Dresselhaus, M.S. Dresselhaus, and M.A. Pimenta, Probing phonon dispersion relations of graphite by double resonance Raman scattering, Physical review letters. 88 (2001) 027401.

[53] J.M. Benoit, J.P. Buisson, O. Chauvet, C. Godon, and S. Lefrant, Low-frequency Raman studies of multiwalled carbon nanotubes: experiments and theory, Physical Review B. 66 (2002) 073417.

[54] S.A. Chernyak, A.S. Ivanov, K.I. Maslakov, A.V. Egorov, Z. Shen, S.S. Savilov, *et al.*, Oxidation, defunctionalization and catalyst life cycle of carbon nanotubes: a Raman spectroscopy view, Phys. Chem. Chem. Phys. 19 (2017) 2276-2285.

[55] S. Maldonado, S. Morin, and K.J. Stevenson, Structure, composition, and chemical reactivity of carbon nanotubes by selective nitrogen doping, Carbon. 44 (2006) 1429-1437.

[56] S. Hussain, R. Amade, E. Jover, and E. Bertran, Nitrogen plasma functionalization of carbon nanotubes for supercapacitor applications, J. Materials Sci. . 48 (2013) 7620–7628.

[57] A. Cuesta, P. Dhamelincourt, J. Laureyns, A. Martinez-Alonso, and J.M.D. Tascón, Raman microprobe studies on carbon materials, Carbon. 32 (1994) 1523-1532.

[58] H. Ago, T. Kugler, F. Cacialli, W.R. Salaneck, M.S.P. Shaffer, A.H. Windle*, et al.*, Work Functions and Surface Functional Groups of Multiwall Carbon Nanotubes, J. Phys. Chem. B. 103 (1999) 8116-8121.